*buildings*

MDPI

*Article*

# On the Boundary Conditions in Out-of-Plane Analysis of Thin Plates by the Finite Point Method

**Sadegh Tavakoliyan [1], Mohamad Najar [1], Parham Memarzadeh [2,*] and Tadeh Zirakian [3]**

[1] Department of Civil Engineering, Isfahan (Khorasgan) Branch, Islamic Azad University, Isfahan 81551-39998, Iran; sadegh.tavakoliyan@khuisf.ac.ir (S.T.); m.najar@khuisf.ac.ir (M.N.)
[2] Department of Civil Engineering, Najafabad Branch, Islamic Azad University, Najafabad 85141-43131, Iran
[3] Department of Civil Engineering and Construction Management, California State University, Northridge, CA 91330, USA; tadeh.zirakian@csun.edu
* Correspondence: p-memar@iaun.ac.ir

**Abstract:** The finite point method (FPM) is a numerical, mesh-free technique for solving differential equations, particularly in fluid dynamics. While the FPM has been previously applied in solid mechanics to analyze plates under in-plane loading, there remains a notable scarcity of research exploring the out-of-plane analysis of elastic plates using this method. This study thoroughly investigates the elastic FPM analysis of thin plates subjected to transverse loadings, focusing specifically on various boundary conditions (BCs). Boundary conditions represent a significant challenge in the out-of-plane analysis of thin plates within the FPM framework. To address this challenge, the approach incorporates additional nodal points positioned close to each boundary node, supplementing the points distributed throughout the plate's interior and along its edges. The strong form of the governing equation is employed for the interior points, while the analysis also includes the scenario of a plate resting on boundary columns. Both distributed and concentrated external loads are examined to provide a comprehensive understanding of the behavior under different loading conditions. Furthermore, the optimal placement of the extra boundary nodes is briefly discussed, alongside a focus on the number of nodes within the finite point clouds. An appropriate range for this number is proposed, although the determination of the optimal distance for the extra boundary nodes and the ideal number of cloud points is earmarked for future research. The contribution of this work is to enhance the understanding of the FPM in the context of thin plates, particularly concerning the critical influence of boundary conditions.

**Keywords:** meshless methods; finite point method; thin plate; boundary conditions; out-of-plane analysis

Academic Editor: Paulo Amado-Mendes

Received: 5 November 2024
Revised: 10 January 2025
Accepted: 13 January 2025
Published: 15 January 2025

**Citation:** Tavakoliyan, S.; Najar, M.; Memarzadeh, P.; Zirakian, T. On the Boundary Conditions in Out-of-Plane Analysis of Thin Plates by the Finite Point Method. *Buildings* **2025**, *15*, 241. https://doi.org/10.3390/buildings15020241



## 1. Introduction

Analysis of thin plates is one of the crucial efforts in structural engineering and mechanics, particularly due to their widespread application in various fields, including aerospace, civil, and mechanical engineering. Traditional methods for analyzing plate behavior, such as the finite element method (FEM), have been extensively developed and implemented. However, these methods often rely on mesh generation and numerical integration, which can introduce complications, particularly in the presence of complex geometries and discontinuities such as shear bands or cracks [1,2].

Recent studies have highlighted the versatility of mesh-free methods. There are several mesh-free methods in the literature including smoothed particle hydrodynamics (SPH) [3,4], the element-free Galerkin (EFG) method [5], and the finite point method (FPM) [6–8]. For instance, Liu et al. (2010) [9] illustrated the application of SPH in solving problems related to fluid–structure interactions, emphasizing its capability to handle complex boundary conditions. Similarly, the EFG method has been modified and employed for various solid mechanics problems, demonstrating its effectiveness in dealing with plate and shell problems [10,11].

The finite point method (FPM), originally developed for applications in fluid dynamics [6,7], emerges as a promising alternative, offering a pure mesh-free framework that simplifies the process of numerical analysis. A series of modifications was applied to the original version of the method increasing its accuracy and eliminating its inefficiencies, which occur due to ill-conditioning of main matrices and divergence. Both original and modified methods are applied successfully for two-dimensional elasticity problems [12–18]. Only a few studies have ventured into solid mechanics, particularly the bending behavior of plates. Recent advancements have begun to address this gap [13,14], but they have not yet addressed utilizing the original version and its main challenges. So, it seems that there is a pressing need to expand the method, especially in its original form for the analysis of plates under transverse loading. Despite its advantages, the flexural analysis of elastic plates using the FPM remains relatively unexplored in the existing literature.

As mentioned before, despite the growing interest in mesh-free methods, the flexural analysis of elastic plates using the FPM remains a relatively under-researched area.

This article aims to fill this gap by presenting a comprehensive study of the finite point method for thin plate analysis. The plate is materially elastic and linear and investigated under different boundary conditions. The strong form of the governing equation, which is a fourth-order differential equation [19,20], is to be satisfied in every internal point, and boundary conditions govern the boundary nodes. Since, according to the governing equilibrium equation, there is only one degree of freedom for nodes, satisfying two components of boundary conditions at border points is the main challenge. There are some techniques to apply more than one boundary condition for nodes located on the boundaries. Lagrange multipliers [21] and the penalty method [22] are the two well-known methods. Similar to the finite difference method, to overcome this problem, we use an extra point in the vicinity of each boundary point. So, the first component of the boundary condition is satisfied using the main boundary node and the other is satisfied using its corresponding extra node [23].

Furthermore, this study investigates the behavior of plates supported on boundary columns, incorporating both distributed and concentrated external loads. The exploration of these configurations aims to enhance the understanding of how boundary conditions affect the stability and accuracy of the FPM analysis. A crucial aspect of our investigation involves determining the optimal distance at which to place the extra boundary nodes and the ideal number of nodes in the finite point clouds, which is essential for achieving reliable results. While preliminary insights are provided, the optimal configurations will be addressed in future research, paving the way for more extensive studies in the field.

Through this work, we hope to contribute to the advancement of mesh-free methodologies in solid mechanics, providing a foundation for future explorations and applications of the finite point method in the analysis of thin plates and discontinuous problems such as crack and shear bands. It is interesting to note that, in the finite point method, the model is created through spreading a set of points as dealing with discontinuity is easier compared to mesh-based methods. So, it seems that the method could be adaptable to problems such as strain softening and crack propagation, which have strong discontinuity. Moreover, expanding the method for vibration of thin plates

with respect to dynamic loads is another intresting field for future studies. In this case, reseaechers will be faced with implementing dynamic equilibrium equations for each point and extracting the stiffness and mass matrices of the plate.

## 2. Thin Plate Theory

In computing stress distribution in a thin plate, the $xy$ plane is placed at its mid-plane. There is a set of logical rules, according to Kirchhoff's hypothesis, as follows:

1. Mid-plane deflection is very small compared to the plate thickness, so the slope of the deflection function is small.
2. The mid-plane after bending is a strain-free surface.
3. The planar surface normal to the mid-plane remains planar and normal to the mid-plane after bending deflection.
4. The stress component normal to the mid-plane is very small compared with other stress components and so can be neglected.

These simplifying rules are similar to simple bending assumptions in beams.

Now consider a small element of this plate under lateral loads. Let the magnitude of element external forces be $p$ and the dimensions of elements be $dx$ and $dy$ along $x$ and $y$ axes, respectively. The displacement field of the plate normal to the mid-plane is denoted by $w$, which is a function with respect to $x$ and $y$ coordinates. Due to pure bending, plate elements rotate around the coordinate axes as

$$\begin{aligned} \theta_x &= \frac{\partial w}{\partial y} \\ \theta_y &= \frac{\partial w}{\partial x} \end{aligned} \tag{1}$$

The curvatures of a deformed surface are defined by differentiation of the slopes with respect to the coordinate axes, which can be written as

$$\begin{aligned} \kappa_x &= \frac{\partial \theta_y}{\partial x} = \frac{\partial^2 w}{\partial x^2} \\ \kappa_y &= \frac{\partial \theta_x}{\partial y} = \frac{\partial^2 w}{\partial y^2} \\ \kappa_{xy} &= \frac{1}{2}\left(\frac{\partial \theta_x}{\partial x} + \frac{\partial \theta_y}{\partial y}\right) = \frac{\partial^2 w}{\partial x \partial y} \end{aligned} \tag{2}$$

As it is described comprehensively in [19,20] and not presented here, bending moment components can be written as follows:

$$\begin{aligned} M_x &= -D\left(\kappa_x + \nu \kappa_y\right) = -D\left(\frac{\partial^2 w}{\partial x^2} + \nu \frac{\partial^2 w}{\partial y^2}\right) \\ M_y &= -D\left(\kappa_y + \nu \kappa_x\right) = -D\left(\frac{\partial^2 w}{\partial y^2} + \nu \frac{\partial^2 w}{\partial x^2}\right) \\ M_{xy} &= -D(1-\nu)\kappa_{xy} = -D(1-\nu)\frac{\partial^2 w}{\partial x \partial y} \end{aligned} \tag{3}$$

in which $D$ is a constant defined as the bending stiffness of the plate,

$$D = \frac{Et^3}{12(1-\nu^2)} \tag{4}$$

Enforcing the shear equilibrium equation along with moment curvature relationships, the governing equation of thin plates can be written as [19]

$$\nabla^4 w = \frac{p}{D} \tag{5}$$

The operator $\nabla^4$ is defined as

$$\nabla^4 = \frac{\partial^4}{\partial x^4} + 2\frac{\partial^4}{\partial x^2 \partial y^2} + \frac{\partial^4}{\partial y^4} \tag{6}$$

The key to finding a thin plate response is to solve Equation (5). However, considering Equation (3), we can have the following equation:

$$M = \frac{M_x + M_y}{1 + \nu} = -D\nabla^2 w \tag{7}$$

So, concerning Equation (5), another solution to thin plate problems is possible by solving the following twin equations:

$$\begin{aligned} \nabla^2 M &= -p \\ \nabla^2 w &= -\frac{M}{D} \end{aligned} \tag{8}$$

in which

$$\nabla^2 = \frac{\partial^2}{\partial x^2} + \frac{\partial^2}{\partial y^2} \tag{9}$$

## 3. Finite Point Method

Due to its resilience, the finite element method (FEM) has been widely adopted as a numerical approach for solving mechanical problems. However, despite this significant advantage, discretizing a model into finite elements can be burdensome. Moreover, the numerical integrations, require to calculate the stiffness matrix and nodal forces, are often time-consuming. To address these drawbacks, a family of methods known as meshless methods has emerged over the past few decades. The primary objective of these methods is to eliminate the need for meshing in mechanical models; however, some variants still require a background mesh for numerical integration. It is important to note that even in cases involving a background mesh, the dependence on meshing is weaker, and as a result creating the meshing process is easier compared to the finite element method.

Based on the above discussion, meshless methods can be classified into two categories: the first class includes methods with a background mesh. These methods utilize numerical integrations and discretize the governing equations based on weak-form formulations. This approach typically results in fewer ill-conditioned system equations, allowing for more accurate results. Although these methods incorporate a mesh, the meshing rules are less stringent than those in the FEM. Notable examples include smoothed particle hydrodynamics and the element-free Galerkin method. The second category of meshless methods contains pure meshless methods. These methods do not use mesh at all, satisfying the strong form of the governing equations over a set of points, thereby eliminating the need for numerical integration. The complete removal of meshing simplifies the creation of mechanical models, and without numerical integration, computational speeds are significantly faster compared to both the first category and the FEM. However, these methods face a higher likelihood of encountering singular matrices, which can compromise the accuracy of the results. The finite point method is a prominent example of this category.

This paper presents a solution for thin plates using the finite point method. The analytical model of the plate is developed by distributing a set of points across the mid-plane. To enforce the governing equations over the points, it is necessary to approximate the primary functions of displacement ($w$) or moments ($M$) in the vicinity of each point. For each point, a relatively small region containing a sufficient number of neighboring nodes is established, known as a "cloud". The point for which the cloud is created is referred to as the "master node". The finite point method approximates objective

functions, applying the weighted least-square method described in [8]. In this approach the objective function $u$ approximated by function $\hat{u}$ is

$$\hat{u} = \boldsymbol{p}^T \boldsymbol{a} \tag{10}$$

in which $\boldsymbol{p}$ is the vector of monomials selected completely or at least symmetrically from the Pascal triangle.

To make the approximated function closely match the function $u$, we first need to identify an error index. This involves calculating the differences between the values of the function $u$ and the values of the approximated function $\hat{u}$ at the cloud points, which we refer to as residuals. The sum of squared residuals across these cloud points serves as the error index. To establish a logical contrast between nodes, we multiply the squared residuals at each point by a weight. The weight is set to 1 at the master node position and decreases monotonically with the distance from the master node. Therefore, the error index can be expressed by the following equation:

$$J = \sum_{i=1}^{n} w(x_i)(\hat{u}_i - u_i)^2 \tag{11}$$

in which $J$ is the error index, $u_i$ is the value of the function $u$ at node $i$, and $w(x_i)$ is the weight at that point. Utilizing (10), the error index can be written as

$$J = \sum_{i=1}^{n} w(x_i)\left(\boldsymbol{p}_i^T \boldsymbol{a} - u_i\right)^2 \tag{12}$$

Minimizing the error index, its derivative with respect to the vector $\boldsymbol{a}$ components must be equal to zero,

$$\frac{\partial J}{\partial \boldsymbol{a}} = 0 \tag{13}$$

resulting in the following equation for the vector $\boldsymbol{a}$:

$$\boldsymbol{a} = \boldsymbol{A}^{-1}\boldsymbol{B}\overline{\boldsymbol{u}} \tag{14}$$

where $\overline{\boldsymbol{u}}$ is the vector of the nodal value of the function $u$ and matrices $\boldsymbol{A}$ and $\boldsymbol{B}$ are defined as follows:

$$\boldsymbol{A} = \sum_{i=1}^{n} w(x_i)\boldsymbol{p}_i\boldsymbol{p}_i^T \tag{15}$$

$$\boldsymbol{B} = \left[w(x_1)\boldsymbol{p}_1 \quad w(x_2)\boldsymbol{p}_2 \quad \cdots \quad w(x_n)\boldsymbol{p}_n\right] \tag{16}$$

Finally, substituting vector $\boldsymbol{a}$ from (14) to (10), the best approximation function is obtained as

$$\hat{u} = \boldsymbol{p}^T\boldsymbol{A}^{-1}\boldsymbol{B}\overline{\boldsymbol{u}} \tag{17}$$

Now there are two different ways to solve thin plate problems. The first is to satisfy twin Equation (8). These equations are generally compatible with plates with simple boundaries. To solve Equation (8), first, the moment parameter $M$ has to be interpolated over clouds and used in the first Equation (8). Then, displacement field $W$ is interpolated and put into the second Equation (8). Finally, the nodal values of the displacement field are obtained. As described above, in this method two separated differential equations with two unknown parameters are satisfied at each node. So, the model behavior is similar to a model with two degrees of freedom for nodes. It is clear that in this case both Dirichlet and Neumann boundary conditions can be enforced similarly to the finite element process.

The second way to solve thin plate problems is to consider Equation (5) as the governing equation. This equation is the general form of the equilibrium equation and

without any limitation can be applied to thin plates with arbitrary boundary conditions. The displacement function, $W$, is interpolated and substituted into Equation (5). As there is only one degree of freedom for nodes, enforcement of boundary conditions is the main challenge. There are different ways to overcome this challenge such as Lagrange multipliers, penalty functions, and using extra nodes. In this paper, the third method is adopted. In this method, an extra node is placed outside the model close to each boundary node. This extra node, along with the main boundary node, acts like a unique boundary node with two degrees of freedom and each one satisfies one of the boundary conditions. This method is exactly similar to what happened in the finite difference method.

## 4. Numerical Examples

First of all, we give a brief description of applying boundary conditions in numerical examples. As mentioned above, a set of additional nodes are placed close to the main boundary nodes, increasing the nodal degrees of freedom in boundaries. So, the main boundary node and its corresponding additional node in total are a two-degree-of-freedom node. The distribution of these additional nodes is shown in Figure 1. Generally, there are two boundary conditions at each boundary node, and now we can satisfy one of them using the main boundary node and the second one at its corresponding additional node. A collection of examples is presented, concentrating on different aspects of plate problems and numerical solutions. Figure 1 represents the general model of a plate in the FPM algorithm, created by spreading a set of points.

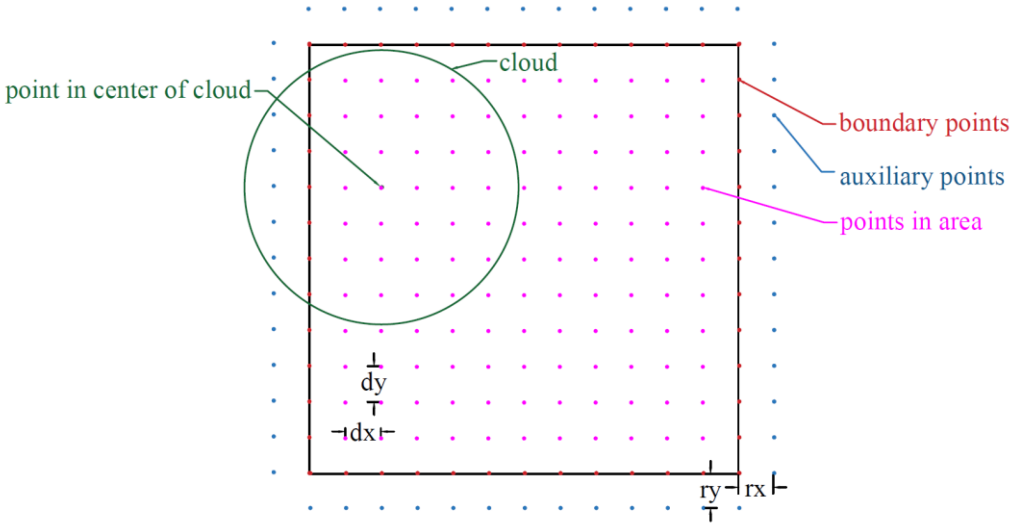


**Figure 1.** Location of auxiliary points.

In Figure 1, $d_x$ and $d_y$ are the horizontal and vertical distance between the main internal nodes of the model, respectively, and $r_x$ and $r_y$ are the horizontal and vertical distance between each additional node and its corresponding main boundary node, respectively.

In the modelling of some plates considered in numerical examples, some mechanical parameters such as modulus of elasticity are considered as unity. Although it is far from the reality from the point of view of an engineer, it is suitable for numerical experiments. Note that in the present work we aimed to invesigate the FPM and search for its drawbacks. The method is applied to linear materials. In this case, the material's properties are considered by selecting its modulus of elasticity and Poisson's ratio. It is clear that if the method performs well for a certain value of modulus of elasticity and Poisson's ratio, it would perform well for any other values of those parameters as well.

So, in investigating the performance of the method, we selected our case studies and their mechanical parameters regardless of their corresponding values in the real world.

**Example 1.** *A simply supported square plate with dimension a = 1 m along both* $x$ *and* $y$ *axes is considered (Figure 2). The plate is affected by a laterally distributed sinusoidal load according to Equation (18).*

$$p(x,y) = qsin\frac{\pi x}{a}sin\frac{\pi y}{a} \tag{18}$$

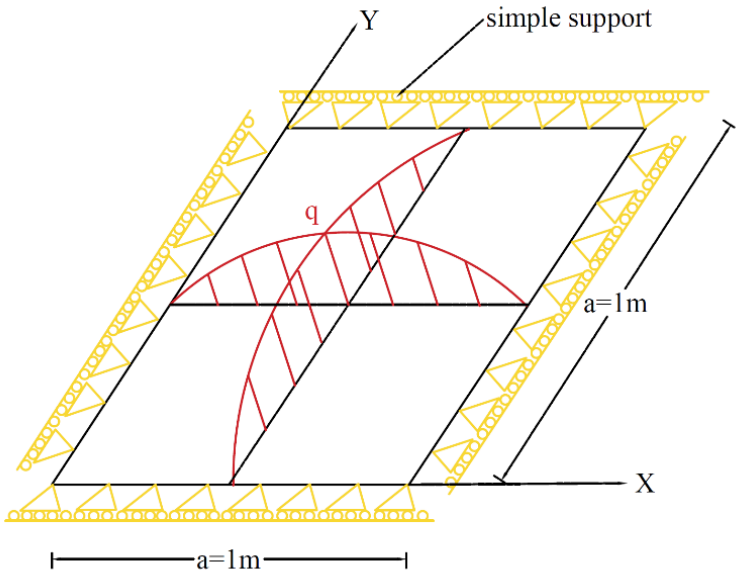


**Figure 2.** Plate under distributed sinusoidal load.

Parameter $q$ is considered to be unity. Simple supports affect boundary nodes, enforcing the following equations:

$$x = 0, x = a \rightarrow w = 0, \frac{\partial^2 w}{\partial x^2} = 0 \tag{19}$$

$$y = 0, y = a \rightarrow w = 0, \frac{\partial^2 w}{\partial y^2} = 0 \tag{20}$$

The analytical exact solution of the problem is presented in [20] as

$$w(x,y) = \frac{qa^4}{4\pi^4 D}sin\frac{\pi x}{a}sin\frac{\pi y}{a} \tag{21}$$

A set of four models is created using different numbers of nodes and solved by applying the finite point method. The displacement surfaces of the models are compared with their corresponding exact surface in Figure 3. As seen, the finite point responses are accurate enough.

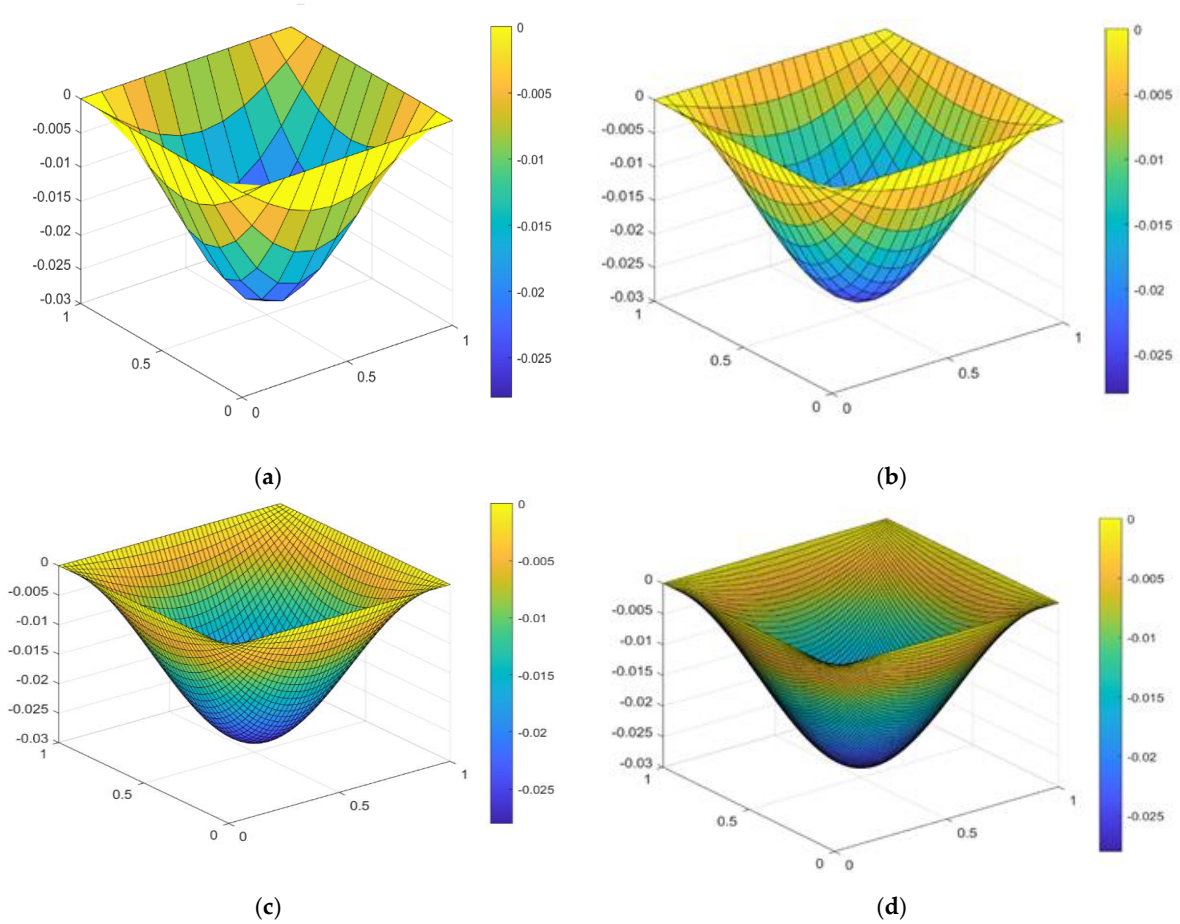


**Figure 3.** Displacement of plate with different numbers of total nodes (FPM). (**a**) 121 points. (**b**) 441 points. (**c**) 2601 points. (**d**) 10,201 points.

The maximum deflections of models calculated by the FPM are compared with the analytical solutions in Table 1. Although it is evident from Table 1 that an increase in points created by the model results in more accuracy, the calculation cost and time might increase significantly.

**Table 1.** Comparison of plate maximum displacement with maximum exact displacement.

| Total Number of Points | Modulus of Elasticity (E) ($kN/m^2$) | Thickness (m) | $Q$ ($kN/m^2$) | Poisson's Ratio $\nu$ | Number of Cloud Points | Number of Monomials | Max Exact (m) | Max FPM (m) |
|---|---|---|---|---|---|---|---|---|
| 121 | 1 | 0.001 | −1 | 0.3 | 30 | 15 | −0.028 | −0.0292 |
| 441 | 1 | 0.001 | −1 | 0.3 | 30 | 15 | −0.028 | −0.0283 |
| 2601 | 1 | 0.001 | −1 | 0.3 | 30 | 15 | −0.028 | −0.0281 |
| 10,201 | 1 | 0.001 | −1 | 0.3 | 30 | 15 | −0.028 | −0.028 |

For a deeper investigation, an error index is defined by Equation (22) over all model points:

$$\text{Convergence rate} = \log \sum \sqrt{\frac{(w_{FPM} - w_{FEM})^2}{n}} \quad (22)$$

The logarithmic graph of the error index versus the total number of points is shown in Figure 4 as the convergence rate. It is clear from the graph that increasing the total number of nodes causes a significant decrease in the error index.

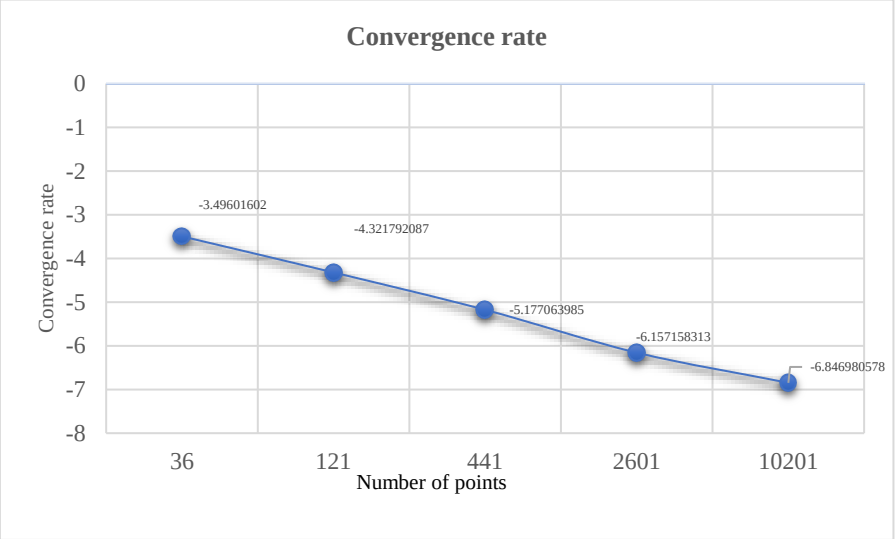


**Figure 4.** Convergence rate.

**Example 2.** *A square plate with simple boundaries is considered against a uniformly distributed lateral load. The area of the load zone is gradually decreased through three different phases and finally converted to a concentrated force. The main problem and the three phases are represented in Figure 5.*

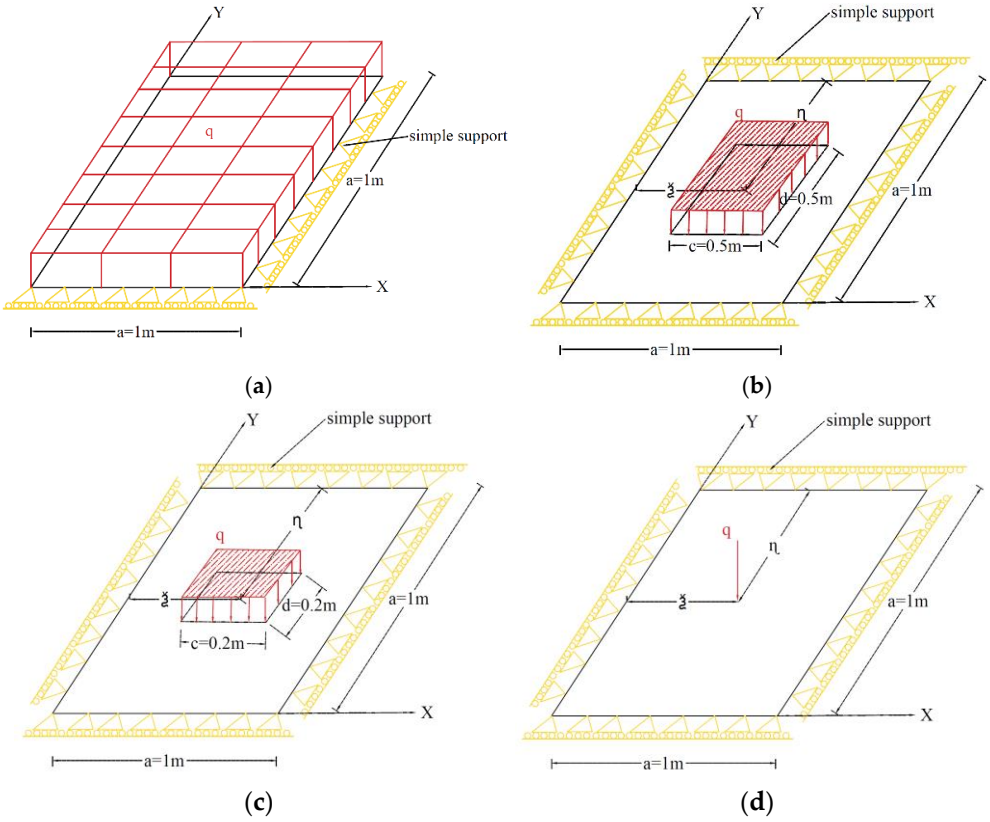


**Figure 5.** (**a**) Main problem plate with uniformly distributed load $q_0$ over whole area; (**b**) plate under uniform load on a quarter of its area at its center; (**c**) plate under uniform load at 4 percent of its area at its center; (**d**) plate under concentrated load.

The exact solutions to these problems are available in [20] as follows:

Case (a):

$$w(x,y) = \sum_{m=1,3,\cdots}^{\infty} \sum_{n=1,3,\cdots}^{\infty} c_{mn} sin\frac{m\pi x}{a} sin\frac{n\pi y}{a} \tag{23}$$

in which

$$c_{mn} = \frac{\frac{16q}{mn\pi^2}}{D\pi^4(\frac{m^2}{a^2}+\frac{n^2}{a^2})} \tag{24}$$

Cases (b,c):

$$w(x,y) = \frac{16q}{\pi^6 D} \sum_{m=1}^{\infty} \sum_{n=1}^{\infty} c_{mn} sin\frac{m\pi x}{a} sin\frac{n\pi y}{a} \tag{25}$$

where

$$c_{mn} = \frac{sin(\frac{m\pi\xi}{a})sin(\frac{n\pi\eta}{a})sin(\frac{m\pi c}{2a})sin(\frac{n\pi d}{2a})}{mn\left[(\frac{m^2}{a^2}+\frac{n^2}{a^2})\right]^2} \tag{26}$$

Case (d):

$$w(x,y) = \frac{4q}{\pi^4 a^2 D} \sum_{m=1}^{\infty} \sum_{n=1}^{\infty} c_{mn} sin\frac{m\pi x}{a} sin\frac{n\pi y}{a} \tag{27}$$

where

$$c_{mn} = \frac{sin(\frac{m\pi\xi}{a})sin(\frac{n\pi\eta}{a})}{\left[(\frac{m^2}{a^2}+\frac{n^2}{a^2})\right]^2} \tag{28}$$

The parameters of Equations (24), (26), and (28) are specified in Figure 5. The lateral load in cases b, c, and d are placed in the center of the plate ($\eta, \xi = 0.5$).

The maximum displacements of the plate in all cases using the FPM are compared with the exact value from analytical solution in Table 2. As is seen from the table, the results from the FPM are close to their exact values.

**Table 2.** Maximum displacement of plate (exact, FPM, and FEM).

| Case | Modulus of Elasticity (E) ($kN/m^2$) | $Q$ ($kN/m^2$) | Poisson's Ratio $\nu$ | Number of Points (FPM) | Number of Nodes for FEM | Number of Elements | Max Exact $w$ (m) | Max FEM $w$ (m) | Max FPM $w$ (m) |
|---|---|---|---|---|---|---|---|---|---|
| a | $1 \times 10^6$ | −1 | 0.3 | 2601 | 2601 | 2500 | −0.04436 | −0.04467 | −0.04439 |
| b | $1 \times 10^6$ | −1 | 0.3 | 2601 | 2601 | 2500 | −0.02328 | −0.02342 | −0.02331 |
| c | $1 \times 10^6$ | −1 | 0.3 | 2601 | 2601 | 2500 | −0.00474 | −0.00477 | −0.00473 |
| d | $1 \times 10^6$ | −1 (kN) | 0.3 | 2601 | 2601 | 2500 | −0.12667 | −0.12759 | −0.12804 |

It is necessary to note that the number of nodes in the finite point model and the finite element model are the same. A close inspection of Figure 6 reveals that when the external load is concentrated, the lateral displacement is concentrated too. In other words, by moving from case a to case d, the blue zone in the displacement graph becomes smaller and smaller.

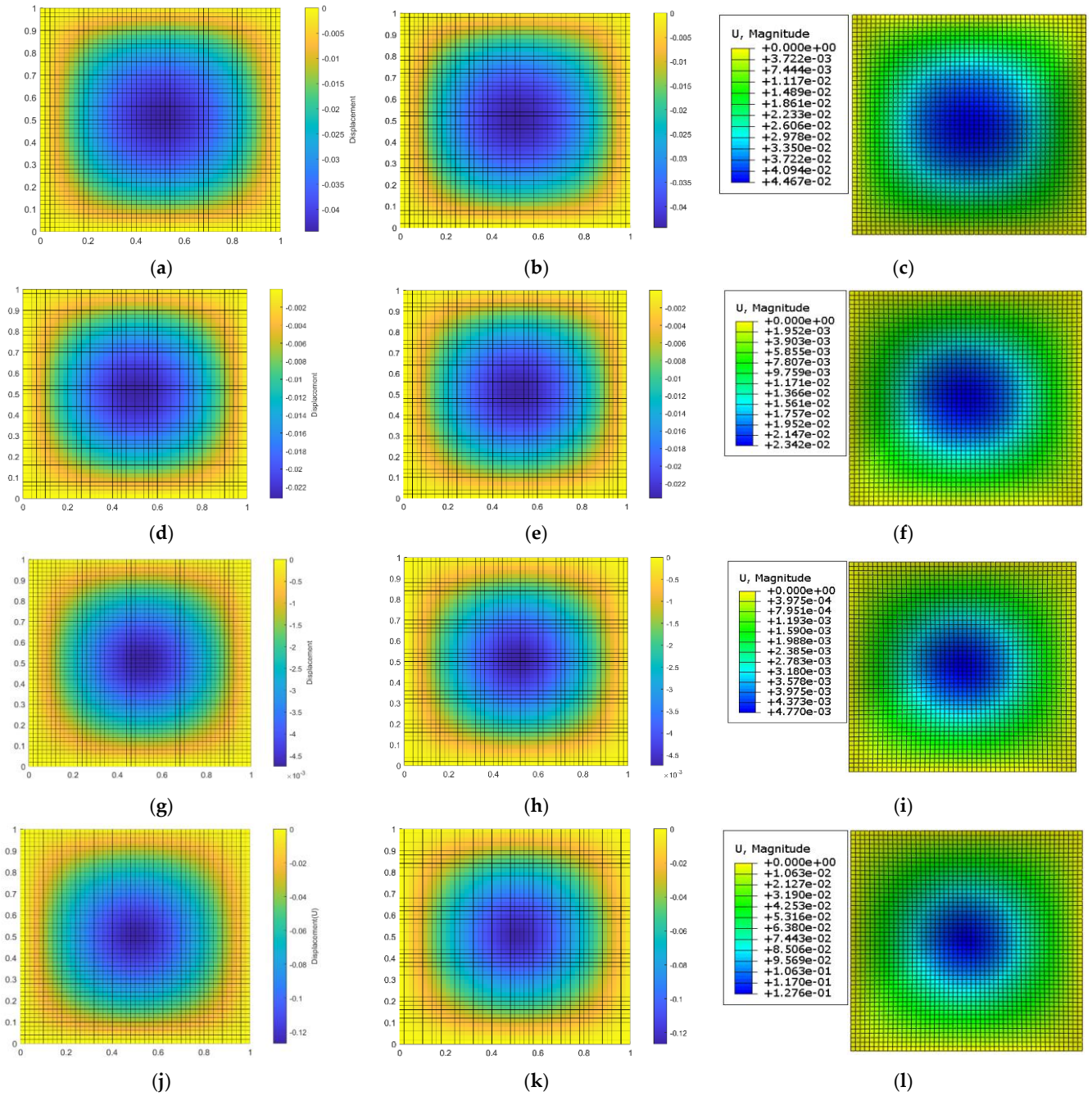


**Figure 6.** Plate response in different phases. (**a**) FPM result in case a. (**b**) Exact result in case a. (**c**) FEM result in case a. (**d**) FPM result in case b. (**e**) Exact result in case b. (**f**) FEM result in case b. (**g**) FPM result in case b. (**h**) Exact result in case b. (**i**) FEM result in case b. (**j**) FPM result in case b. (**k**) Exact result in case b. (**l**) FEM result in case b.

The error index introduced by Equation (22) is applied to these four problems in the finite point and the finite element solutions and the results are plotted in Figure 7. It is clear from the graph that in some cases far from concentrated loads, the finite point method leads to more exact solutions; however, in the cases close to concentrated loads, the finite element method surpassed the finite point solution.

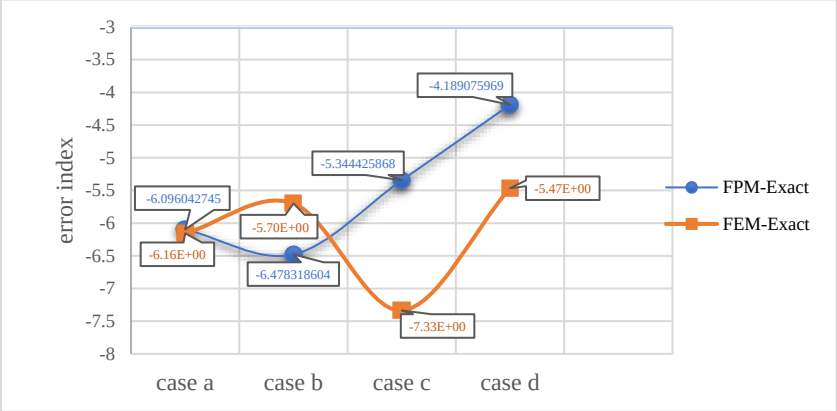


**Figure 7.** Comparison of the error index of FEM and FPM methods to the exact solution.

**Example 3.** *In this section, again the square plate of the previous problem is considered, but a variety of different boundary conditions are applied to its borders. The solution is focused on the number of cloud points and aims to see its effect on the accuracy of the calculated response. The plate is under a uniform distributed load and is investigated in three different cases as below.*

In case a, three border lines are restrained by simple supports, and the fourth one is fixed. In case b, two parallel borders are hinged and the others are fixed, and finally, in case c, all borders are fixed. These three cases are shown in Figure 8.

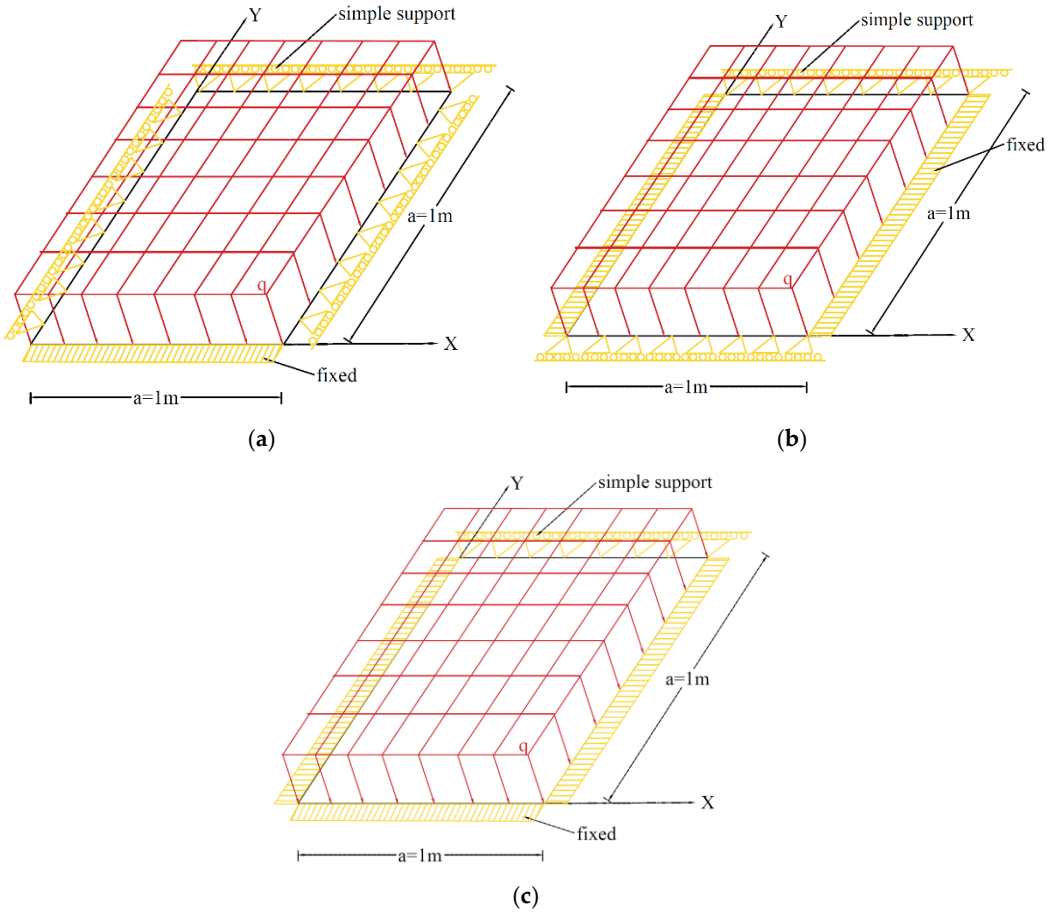


**Figure 8.** Plate under uniform distributed load: (**a**) plate with fixed support along one edge and simple supports along the other edges; (**b**) plate with fixed supports along two parallel edges and simple supports along the other edges; (**c**) plate with fixed supports along three edges and a simple support along the other edge.

The exact solution of these three problems is reported in [20] as follws:

$$case\ a\ \Rightarrow w_{exact\,(x\,=\,0.5,y\,=\,0.5)}\ =\ 0.00280\frac{qa^4}{D} \tag{29}$$

$$case\ b\ \Rightarrow w_{exact\,(x\,=\,0.5,y\,=\,0.5)}\ =\ 0.00192\frac{qa^4}{D} \tag{30}$$

$$case\ c\ \Rightarrow w_{exact\,(x\,=\,0.5,y\,=\,0.5)}\ =\ 0.00126\frac{qa^4}{D} \tag{31}$$

The contrast between the simple and fixed supports is obvious in Figure 9.

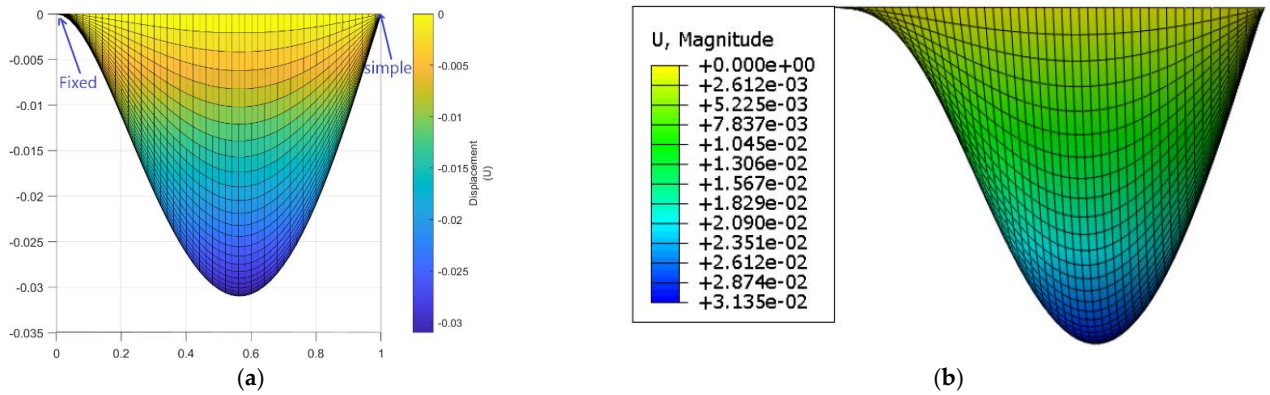


(**a**) (**b**)

**Figure 9.** Displacement of case a in *x*–*z* plane: (**a**) FPM, (**b**) FEM.

Table 3 shows the maximum displacement for problem cases a, b, and c calculated by analytical exact relations, the finite element method, and the finite point method. The plate is modelled in both the finite element and finite point methods spreading 2601 points. The finite point procedure runs five times with different numbers of points in clouds equal to 15, 30, 40, 60, and 90, respectively. As a mathematical obligation, the number of cloud points must be greater than the number of monomials, so the minimum number of cloud points is considered equal to the number of monomials. It is clear from Table 3 that increasing the number of cloud points up to 60 results in an increase in accuracy, but further increase in the number of cloud points leads to instability and so reduces the accuracy.

The displacement of plate case c calculated by the finite point method with 90 and 30 cloud points is shown in Figure 10. The instability of calculations is obvious in the case of 90 points in the clouds. There is a need, in future studies, to determine the optimum number of cloud points.

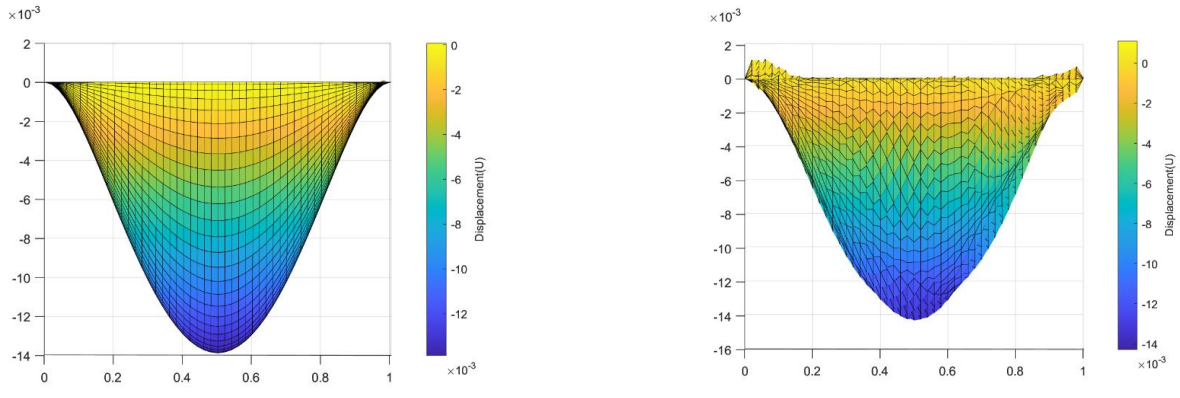


(**a**) (**b**)

**Figure 10.** Displacement of case c with FPM: (**a**) 30 points in cloud, (**b**) 90 points in cloud.

**Table 3.** Displacement at plate center: exact, FEM, and FPM with various numbers of cloud points.

| Case | Modulus of Elasticity (E) ($kN/m^2$) | $q$ ($kN/m^2$) | Poisson's Ratio $\nu$ | Number of Points (FPM) | Number of Elements (FEM) | Number of Points in Cloud | Exact in $x$ = 0.5, $y$ = 0.5 $w$ (m) | FEM in $x$ = 0.5, $y$ = 0.5 $w$ (m) | FPM in $x$ = 0.5, $y$ = 0.5 $w$ (m) |
|---|---|---|---|---|---|---|---|---|---|
| a | $1 \times 10^6$ | −1 | 0.3 | 2601 | 2500 | 15 | −0.030576 | −0.030566 | −0.033853 |
| a | $1 \times 10^6$ | −1 | 0.3 | 2601 | 2500 | 30 | −0.030576 | −0.030566 | −0.034115 |
| a | $1 \times 10^6$ | −1 | 0.3 | 2601 | 2500 | 40 | −0.030576 | −0.030566 | −0.030275 |
| a | $1 \times 10^6$ | −1 | 0.3 | 2601 | 2500 | 60 | −0.030576 | −0.030566 | −0.030554 |
| a | $1 \times 10^6$ | −1 | 0.3 | 2601 | 2500 | 90 | −0.030576 | −0.030566 | −0.031118 |
| b | $1 \times 10^6$ | −1 | 0.3 | 2601 | 2500 | 15 | −0.021012 | −0.020998 | −0.017826 |
| b | $1 \times 10^6$ | −1 | 0.3 | 2601 | 2500 | 30 | −0.021012 | −0.020998 | −0.023643 |
| b | $1 \times 10^6$ | −1 | 0.3 | 2601 | 2500 | 40 | −0.021012 | −0.020998 | −0.021118 |
| b | $1 \times 10^6$ | −1 | 0.3 | 2601 | 2500 | 60 | −0.021012 | −0.020998 | −0.020996 |
| b | $1 \times 10^6$ | −1 | 0.3 | 2601 | 2500 | 90 | −0.021012 | −0.020998 | −0.022524 |
| c | $1 \times 10^6$ | −1 | 0.3 | 2601 | 2500 | 15 | −0.013759 | −0.013846 | −0.019428 |
| c | $1 \times 10^6$ | −1 | 0.3 | 2601 | 2500 | 30 | −0.013759 | −0.013846 | −0.014354 |
| c | $1 \times 10^6$ | −1 | 0.3 | 2601 | 2500 | 40 | −0.013759 | −0.013846 | −0.013752 |
| c | $1 \times 10^6$ | −1 | 0.3 | 2601 | 2500 | 60 | −0.013759 | −0.013846 | −0.013831 |
| c | $1 \times 10^6$ | −1 | 0.3 | 2601 | 2500 | 90 | −0.013759 | −0.013846 | −0.014298 |

The displacement responses for problems cases a, b, and c along $x = 0.5$ in FEM and FPM procedures are compared in Figures 11, 12, and 13, respectively. As mentioned above, there are acceptable adjustments between FEM and FPM responses with up to 60 points in the clouds. As seen in Figure 14, with further increasing the number of points in clouds, the error index climbs up gradually.

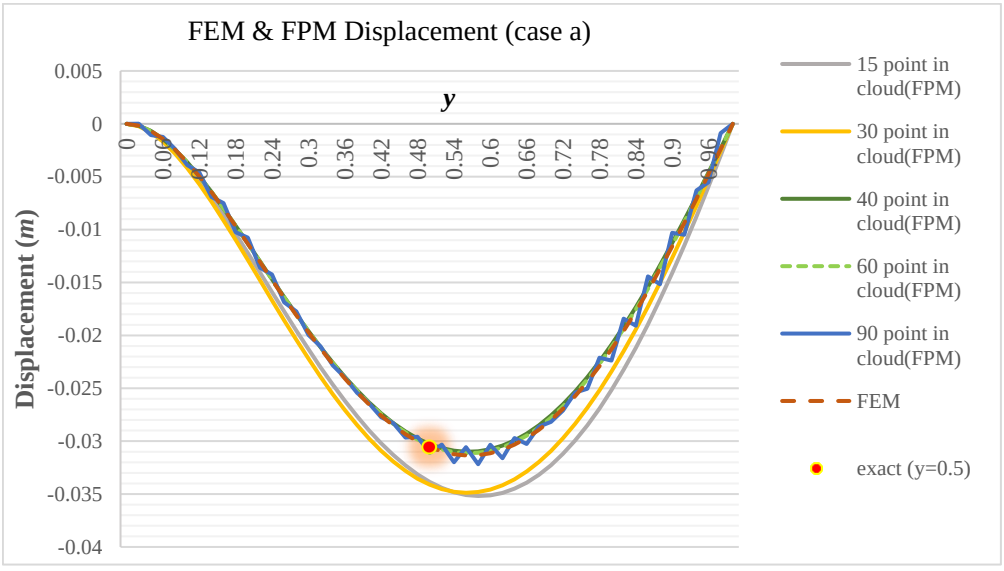


**Figure 11.** Displacement of plate case a along $x = 0.5$.

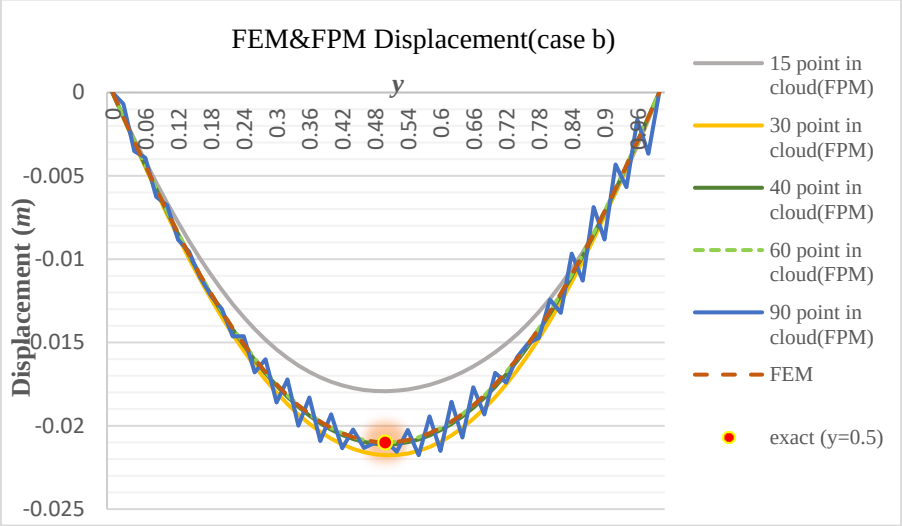


**Figure 12.** Displacement of plate case b along $x = 0.5$.

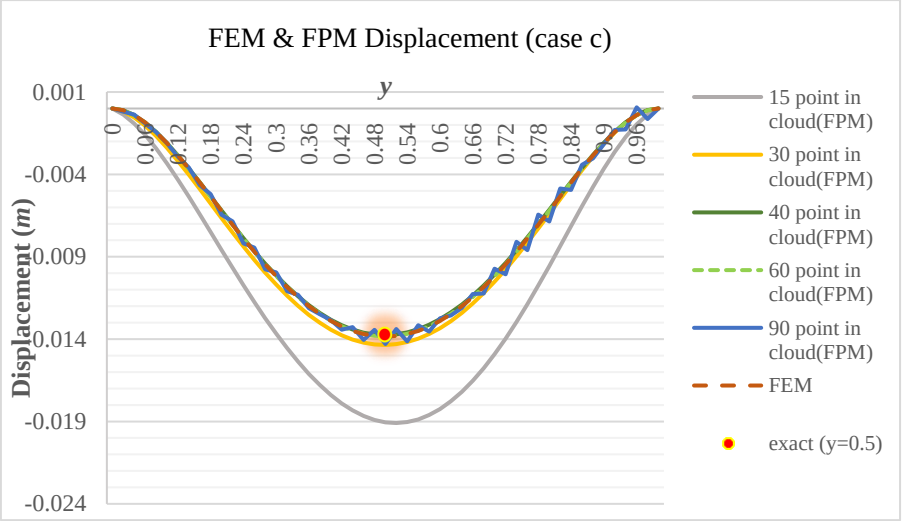


**Figure 13.** Displacement of plate case c along $x = 0.5$.

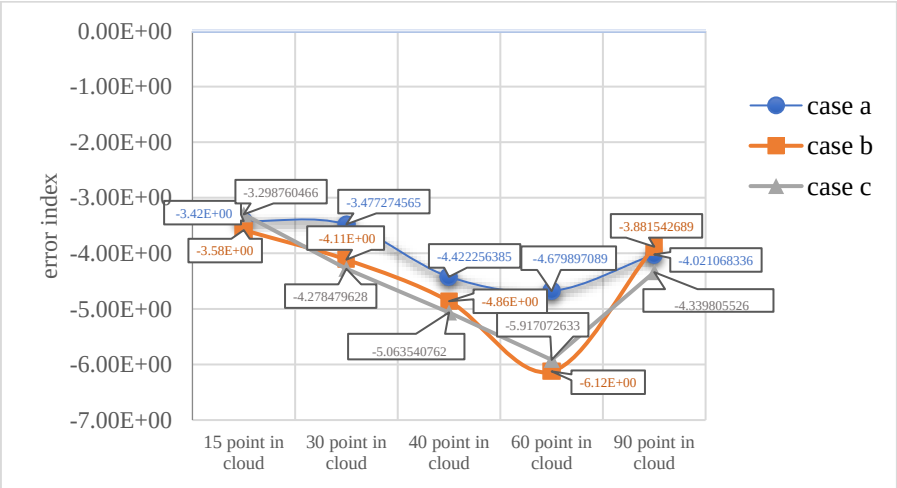


**Figure 14.** Comparison of error indexes for FPM and FEM in cases a, b, and c.

**Example 4.** *The square plate with dimension a = 1 m is again considered. The plate is under two different boundary conditions. In the first one (case a), two parallel borders are fixed and the two others are simple, while in the second (case b), all borders are fixed. As is shown in Figure 15, the*

*plate is affected by a linear triangular distributed load along the* $y$ *axis, and a constant load along the x axis. So, the equation of external load can be written as follows:*

$$Q(x,y) = \frac{qy}{a} \tag{32}$$

In this section, the focus is on the position and distance of additional boundary nodes from the plate borders. The maximum displacement of the plate with fixed supports (case b) is given in [20] as

$$w_{max} = 0.00126\frac{qa^4}{D} \tag{33}$$

As shown in Figure 16, in both finite element and finite point solutions, the blue area is more elongated in the direction of the simple supports, which is acceptable behavior.

In both Figures 16 and 17, the point with maximum displacement has shifted to the left, which is due to the entry of the maximum triangular load on the left boundary.

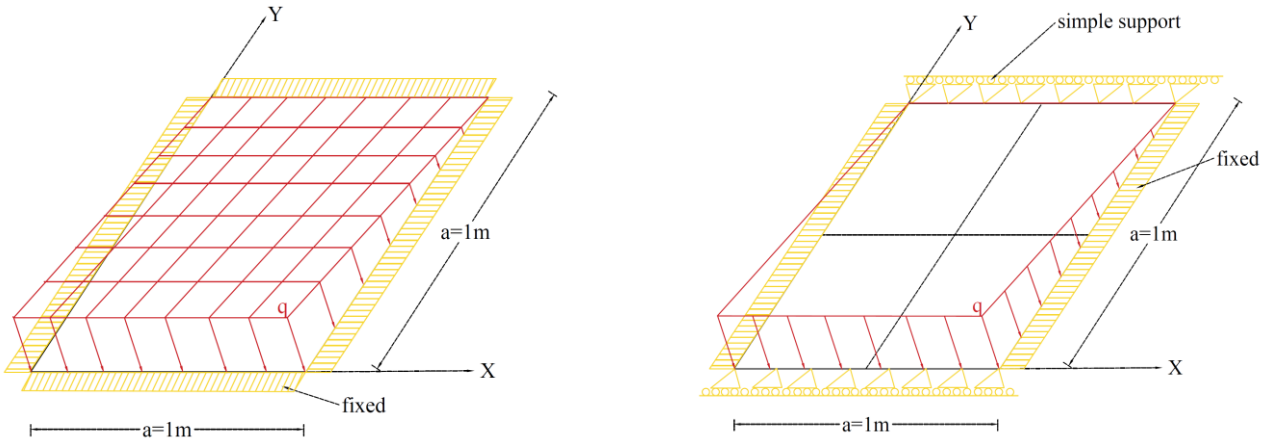


**Figure 15.** Plate with a distributed triangular load.

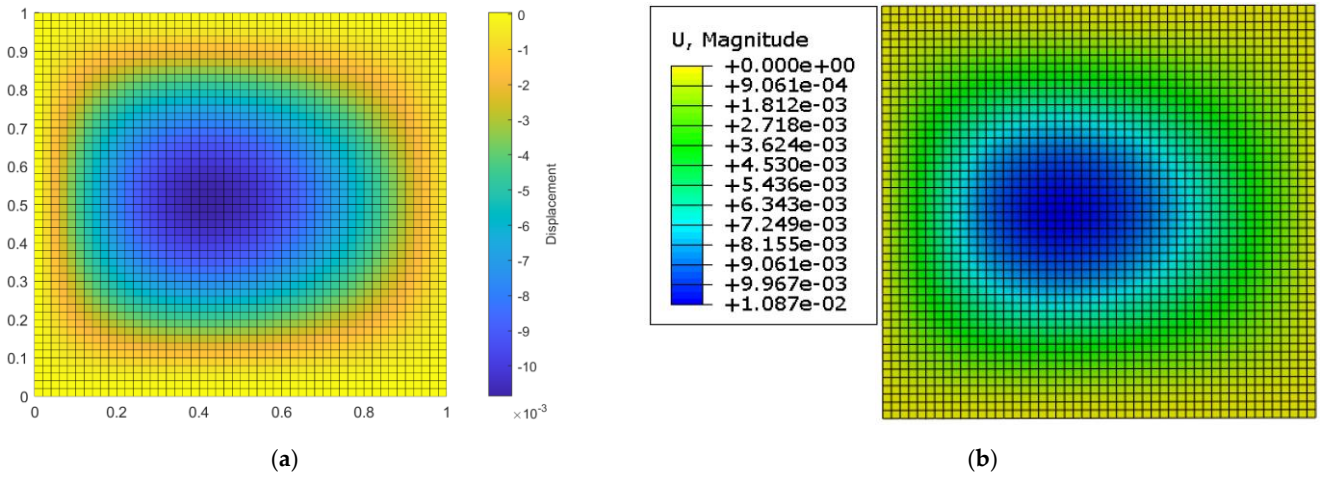


**Figure 16.** Displacement response of plate case a: (**a**) FEM, (**b**) FPM.

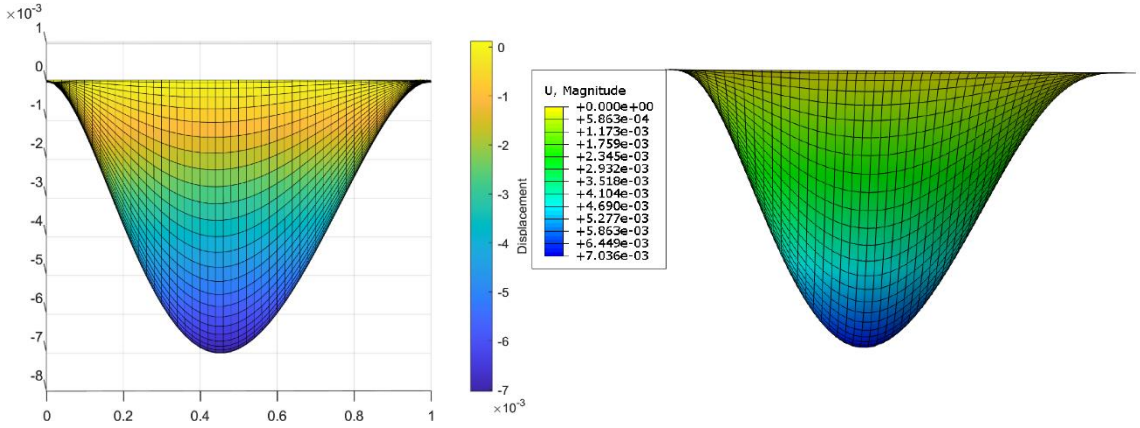


(**a**) (**b**)

**Figure 17.** Displacement response of plate case a (*x*–*z* axis): (**a**) FEM, (**b**) FPM.

In Table 4, the centroid displacements of the plate in cases a and b are presented from the exact solution, the FEM, and the FPM, respectively. It is clear from the table that when additional point distances from borders are about the general point distances and higher, large errors occur. By decreasing the distance of additional nodes from borders, the numerical errors are reduced. However, in the case of too small a distance, the stiffness matrix moves rapidly toward singularity.

**Table 4.** Displacement at plate center in cases a and b for additional nodes at various distance from borders.

| Case | Modulus of Elasticity (E) ($kN/m^2$) | $Q$ ($kN/m^2$) | Poisson's Ratio $\nu$ | Distance of Point (FPM) (m) | Distance of Point (FEM) (m) | Distance of Auxiliary Points (m) ($r_x = r_y$) | Exact in $x$ = 0.5, $y$ = 0.5 $w$ (m) | FEM in $x$ = 0.5, $y$ = 0.5 $w$ (m) | FPM in $x$ = 0.5, $y$ = 0.5 $w$ (m) |
|---|---|---|---|---|---|---|---|---|---|
| a | $1 \times 10^6$ | −1 | 0.3 | 0.02 | 0.02 | 0.2 | −0.010855 | −0.010873 | −3079.511 |
| a | $1 \times 10^6$ | −1 | 0.3 | 0.02 | 0.02 | 0.02 | −0.010855 | −0.010873 | −0.012378 |
| a | $1 \times 10^6$ | −1 | 0.3 | 0.02 | 0.02 | 0.002 | −0.010855 | −0.010873 | −0.011013 |
| a | $1 \times 10^6$ | −1 | 0.3 | 0.02 | 0.02 | 0.0002 | −0.010855 | −0.010873 | −0.010888 |
| a | $1 \times 10^6$ | −1 | 0.3 | 0.02 | 0.02 | 0.00002 | −0.010855 | −0.010873 | −0.010867 |
| b | $1 \times 10^6$ | −1 | 0.3 | 0.02 | 0.02 | 0.2 | −0.006879 | −0.007035 | −933.8225 |
| b | $1 \times 10^6$ | −1 | 0.3 | 0.02 | 0.02 | 0.02 | −0.006879 | −0.007035 | −0.008163 |
| b | $1 \times 10^6$ | −1 | 0.3 | 0.02 | 0.02 | 0.002 | −0.006879 | −0.007035 | −0.007134 |
| b | $1 \times 10^6$ | −1 | 0.3 | 0.02 | 0.02 | 0.0002 | −0.006879 | −0.007035 | −0.007038 |
| b | $1 \times 10^6$ | −1 | 0.3 | 0.02 | 0.02 | 0.00002 | −0.006879 | −0.007035 | −0.007029 |

Figure 18 represents the error index of FPM models with different distances for additional boundary points by considering the finite element results as the exact solution. As a primary obligation, it is noted from the results that the additional node distance from the plate border must be about and greater than the distance between general points.

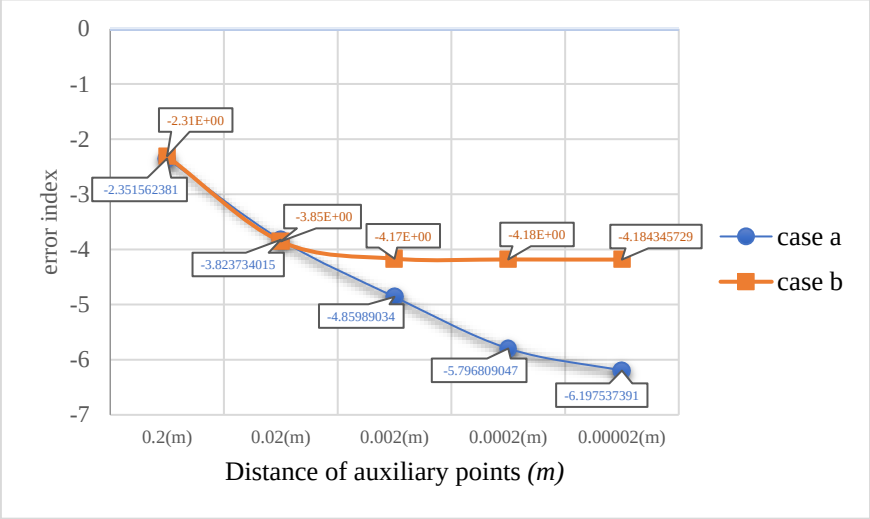


**Figure 18.** Comparison of the error index in FPM compared to FEM.

**Example 5.** *The square plate with dimension a = 1 m is considered. The border along the* $y$ *axis is fixed and the two others are simple. As shown in Figure 19, a distributed load that is sinusoidal along the* $y$ *axis and constant along the x axis is applied to the plate. The external load equation can be written as follows:*

$$0 \le x \le a \rightarrow Q = q \tag{34}$$

$$0 \le y \le a \rightarrow Q = qsin\frac{\pi y}{a} \tag{35}$$

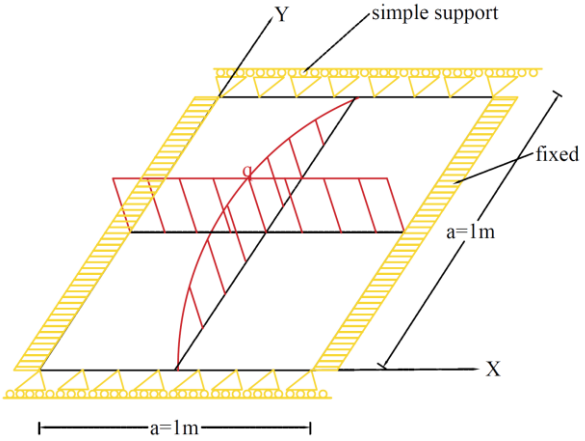


**Figure 19.** Plate with simple and fixed supports under lateral load.

The maximum displacement of the plate is calculated analytically in [20] as follows:

$$w_{max} = w\left(\frac{a}{2}, 0\right) = 0.00154\frac{qa^4}{D} \tag{16}$$

The displacement response of the plate from the FPM is compared to that from the FEM in Figure 20. In Table 5 the maximum displacement of the plate is compared in three cases (exact, FEM, and FPM). To evaluate the effect of the weight function, numerical calculations were repeated without applying the weights. As shown in Table 5, the numerical error increased in this case. The displacement response of the plate along $x = 0.5$ is also plotted for different cases in Figure 21.

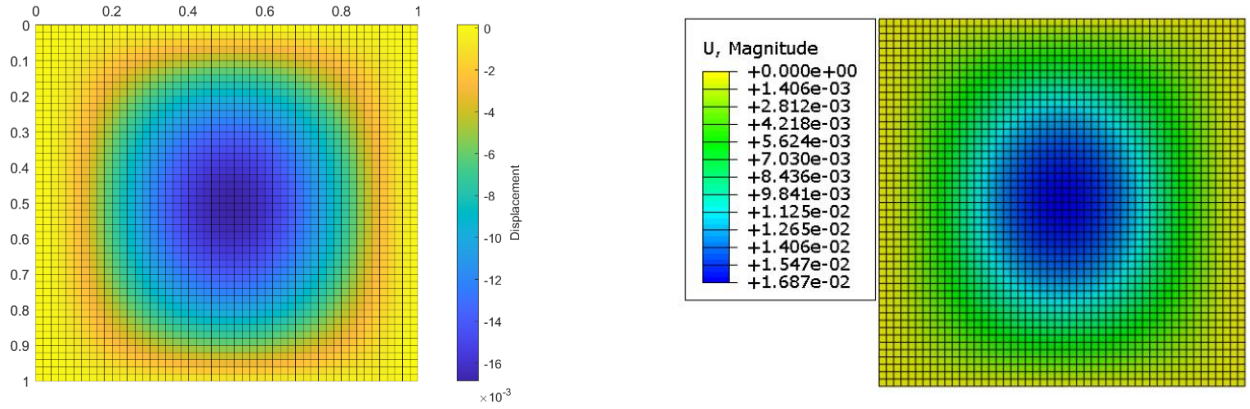


(**a**) (**b**)

**Figure 20.** Plate displacement: (**a**) FPM, (**b**) FEM.

**Table 5.** Comparison of maximum displacement: exact, FEM, and FPM.

| Modulus of Elasticity (E) ($kN/m^2$) | $q$ ($kN/m^2$) | Poisson's Ratio $\nu$ | Distance of Point (FPM) (m) | Distance of Point (FEM) (m) | Weight Function | Exact in $x$ = 0.5, $y$ = 0.5 $w$ (m) | FEM in $x$ = 0.5, $y$ = 0.5 $w$ (m) | FPM in $x$ = 0.5, $y$ = 0.5 $w$ (m) | Convergence Rate Between FPM & Exact (All Points) |
|---|---|---|---|---|---|---|---|---|---|
| $1\times 10^6$ | −1 | 0.3 | 0.02 | 0.02 | Off | −0.016826 | −0.016871 | −0.020419 | 0.0003311 |
| $1\times 10^6$ | −1 | 0.3 | 0.02 | 0.02 | On | −0.016826 | −0.016871 | −0.016850 | $3.605\times 10^{-6}$ |

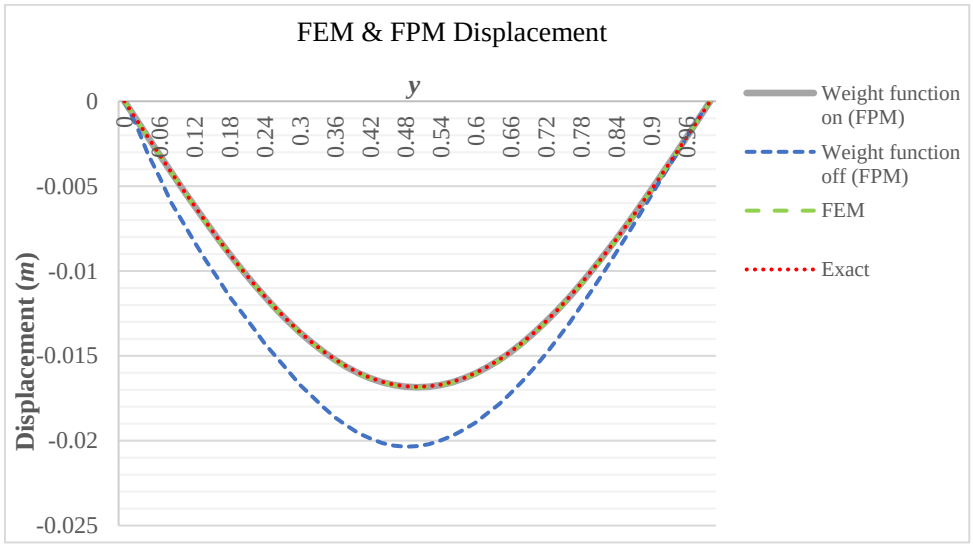


**Figure 21.** Displacement of the plate along $x = 0.5$.

**Example 6** *The square plate of the previous section is considered and one of its fixed supports is removed. So, its borders along the* $y$ *axis are supported simply, one along the* $x$ *axis is fixed, and the other one along* $x$ *axis is free. The plate is under a uniform distributed load with an intensity equal to* $q$*. The plate is shown in Figure 22.*

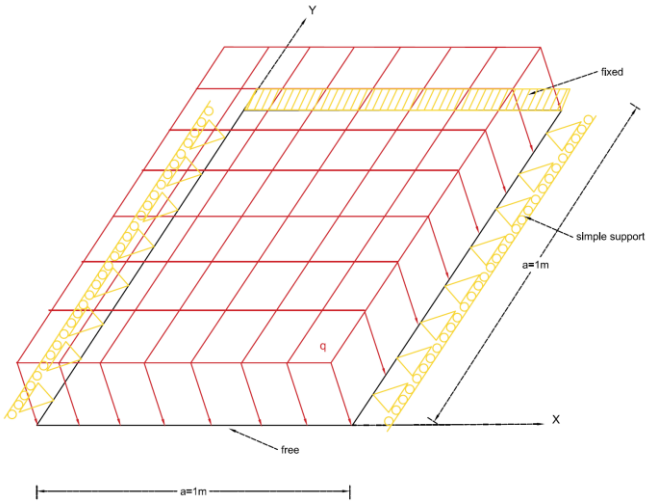


**Figure 22.** Plate with three kinds of support conditions under uniform load.

The maximum displacement of the plate by solving the governing differential equation exactly is given in [20] as

$$w_{max} = 0.0113\frac{qa^4}{D} \tag{17}$$

The displacement response of the plate calculated by the FPM and the FEM are plotted in Figure 23 and can be compared. The maximum displacement from these two methods and the exact value are also listed in Table 6. The displacement response of the plate along $y = 0.5$ is also plotted in Figure 24.

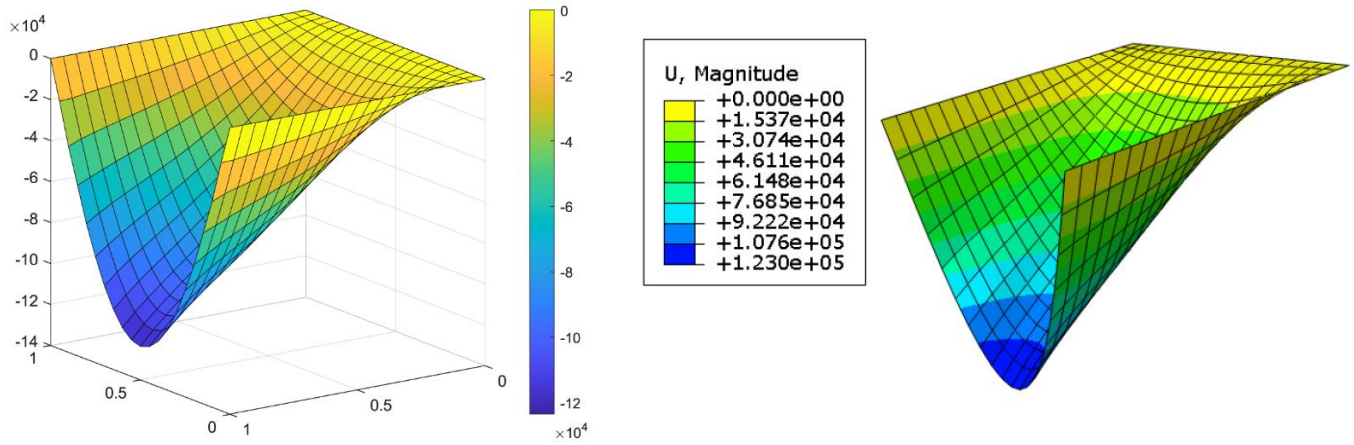


(**a**) (**b**)

**Figure 23.** Plate displacement response: (**a**) FPM, (**b**) FEM.

**Table 6.** Maximum displacement (exact, FEM, and FPM).

| Method | Modulus of Elasticity (E) ($kN/m^2$) | $q$ ($kN/m^2$) | Poisson's Ratio $\nu$ | Number of Points or Elements | Max Exact (m) | Max (m) | Percent Error |
|---|---|---|---|---|---|---|---|
| FPM | $1\times 10^6$ | −1 | 0.3 | 441 | −0.1234 | −0.1236 | 0.162 |
| FEM (shell4R) | $1\times 10^6$ | −1 | 0.3 | 400 | −0.1234 | −0.1229 | 0.405 |

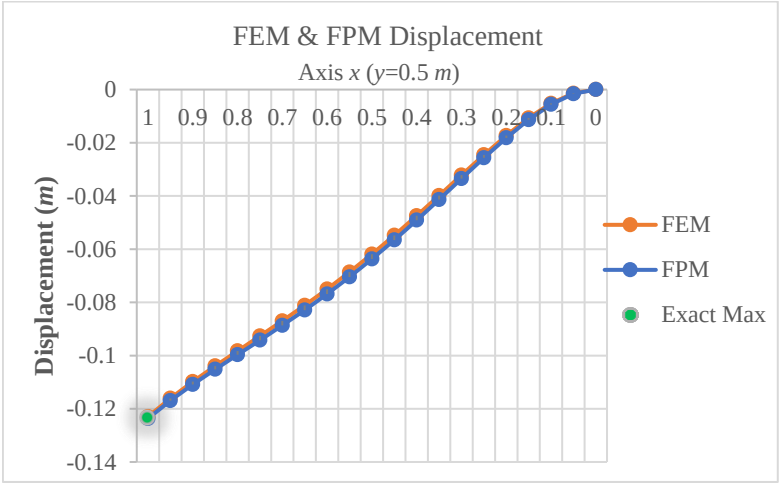


**Figure 24.** Displacement response of plate with three kinds of support conditions along $y = 0.5$.

**Example 7.** *The square plate from the previous problems is considered over columns at its corners and is affected by a uniform distributed load. The plate is shown in Figure 25.*

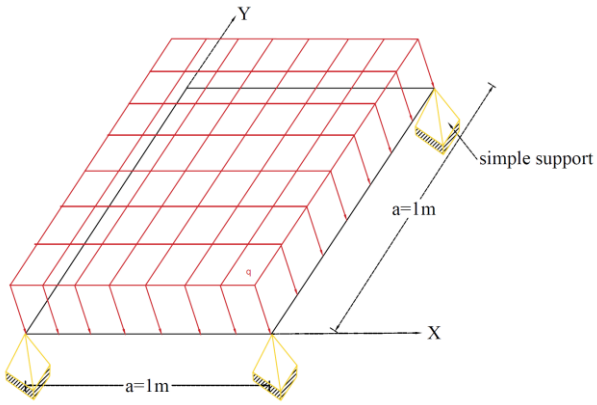


**Figure 25.** Plate over corner columns and under uniform distributed load.

The displacement response of the plate calculated by the finite point and the finite element methods is plotted in Figure 26 and its displacement along $y = 0.5$ is shown in Figure 27. The finite point response is close to the finite element response.

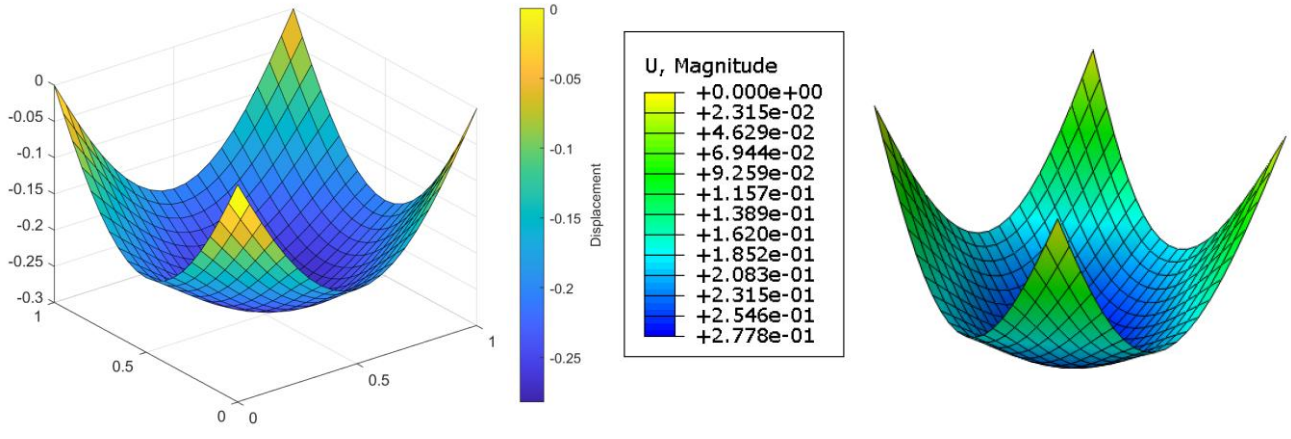


(**a**) (**b**)

**Figure 26.** Displacement response of the plate: (**a**) FPM, (**b**) FEM.

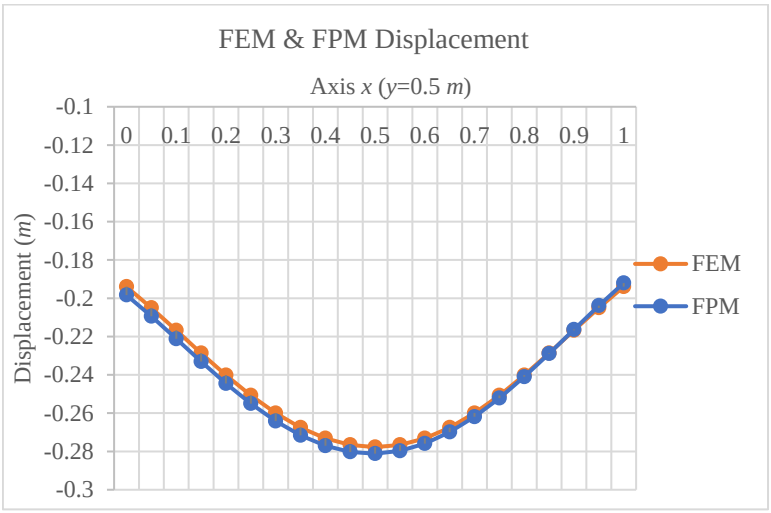


**Figure 27.** Displacement response of plate over corner columns along $y = 0.5$.

**Example 8.** *The square plate from the previous problems, with one fixed support along the* $x$ *axis and three other borders without support are considered and affected by a uniform distributed load. The plate is shown in Figure 28.*

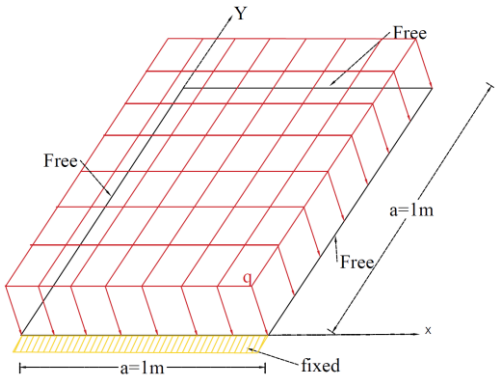


**Figure 28.** Plate with a fixed support and three free boundaries under constant distributed load.

The displacement response of the plate calculated with the finite point and finite element procedures is shown in Figure 29 and the displacement along $y = 0.5$ is plotted in Figure 30.

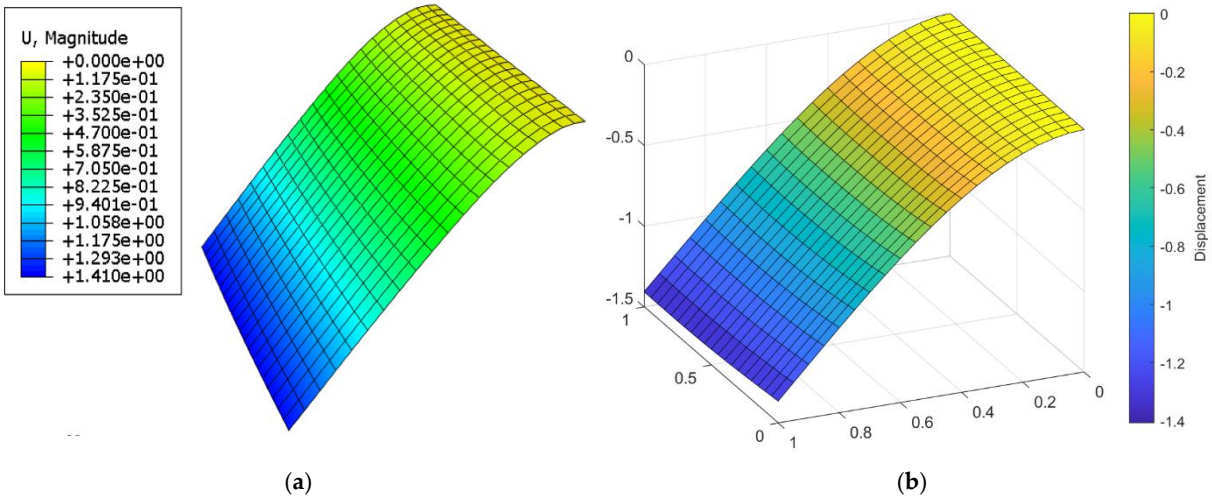


(**a**) (**b**)

**Figure 29.** Displacement response: (**a**) FEM, (**b**) FPM.

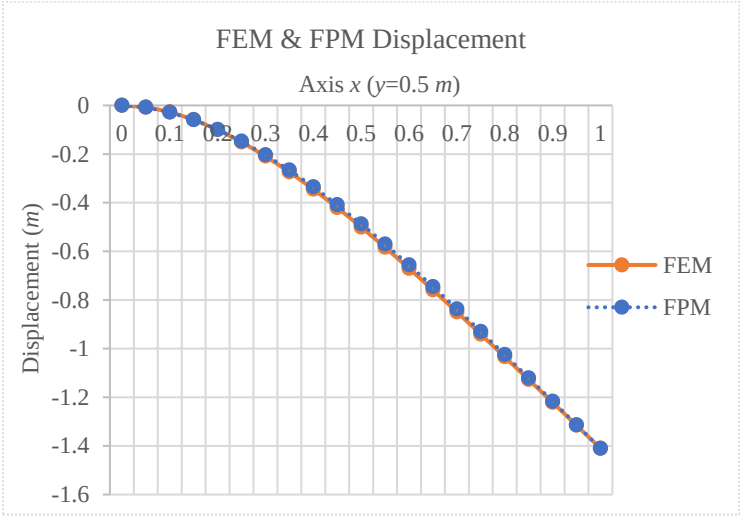


**Figure 30.** Comparison of the approximate value of the solution by the FEM and the FPM.

## 5. Conclusions

In this article, the finite point method was applied to the out-of-plane analysis of thin plates. Note that, although a number of scientific works have applied the finite point method for two-dimensional in-plane problems, and there are powerful modified and promoted versions of the method in those cases, there is still a pressing need to investigate the method for three-dimensional bending problems. This paper aimed to apply the original version of the finite point method to thin plate problems as a threshold for future developments of the method. Several plates with different mechanical properties, such as a variety of support conditions including column boundaries subjected to a wide range of external loads from uniformly distributed to linear, harmonic and concentrated, are considered for a deep inspection of the method, revealing its hidden drawbacks. The meshless nature of the finite point method simplifies the creation of numerical models compared to mesh-based methods. This approach is particularly useful for problems involving strong discontinuities, such as strain softening and crack propagation, as nodes can be arranged along the discontinuity paths. This avoids the time-consuming task of mesh refinement. Besides these breathtaking aspects, satisfying boundary conditions is the main challenge even in elastic linear tasks as there is only one degree of freedom for model points. In this paper, drawing inspiration from the finite difference method, we satisfy the boundary conditions. Numerical models were constructed by distributing regular mesh points across the plates and their borders. The finite point method was then applied, and the resulting model responses were compared to analytical solutions when available. In cases lacking analytical responses, finite element models were created using the same number of points as in the finite point model for comparison. The numerical error index was calculated for each case and yielded satisfactory results across the board.

Initially, this method was investigated in the context of linear elastic thin plates. A series of rectangular plates with various boundary conditions were analyzed, incorporating different combinations of simple, fixed, and free boundary conditions under various external loads. In one case study, a plate was supported by four rigid columns, while in another, a distributed external load was gradually concentrated. A deeper investigation focused on the distance between boundary nodes and their corresponding extra nodes. When these distances were small or comparable to those between internal nodes, the results remained accurate. However, greater distances led to significant numerical errors. The number of nodes within interpolation clouds was also examined, revealing that a

commonly used number of cloud nodes produced results close to benchmarks. In contrast, using too few or too many cloud nodes resulted in numerical instability.

This study represents a preliminary application of the finite point method to plate problems, which can be seen as a starting point in developing the method for application to a great range of mechanical problems. As the method succeeded in solving the linear thin plates it is now the time to determine the method parameters such as the number of cloud points and also evaluate the method's robustness for nonlinear problems in future research.

**Author Contributions:** Conceptualization, M.N. and P.M.; Methodology, M.N.; Software, S.T.; Validation, M.N., P.M. and T.Z.; Resources, T.Z.; Writing—original draft, S.T.; Writing—review & editing, M.N., P.M. and T.Z.; Supervision, M.N. and P.M. All authors have read and agreed to the published version of the manuscript.

**Funding:** This research received no external funding.

**Data Availability Statement:** Data are contained within the article.

**Conflicts of Interest:** The authors declare no conflict of interest.

## References

1. Saberi, S.; Memarzadeh, P.; Zirakian, T. Study of buckling stability of cracked plates under uniaxial compression using singular FEM. *Struct. Eng. Mech. Int J.* **2019**, *69*, 417–426.
2. Taheri, M.H.; Memarzadeh, P. Experimental and numerical study of compressive buckling stability of plates with off-center crack. *Theor. Appl. Fract. Mech.* **2020**, *109*, 102706.
3. Monaghan, J.J. Smoothed particle hydrodynamics. *Annu. Rev. Astron. Astrophys.* **1992**, *30*, 543–574.
4. Monaghan, J.J. Smoothed particle hydrodynamics. *Rep. Prog. Phys.* **2005**, *68*, 1703.
5. Belytschko, T.; Lu, Y.; Gu, L. Element free Galerkin Methods. *Int. J. Numer. Methods Eng.* **1994**, *37*, 229–256.
6. Onate, E.; Idelson, S.; Zienkiewicz, O.C.; Taylor, R.L. A finite point method in computational mechanics applications to convective transport and fluid flow. *Int. J. Numer. Methods Eng.* **1996**, *39*, 3839–3866.
7. Onate, E.; Idelson, S.; Zienkiewicz, O.C.; Taylor, R.L. A stabilized finite point method for analysis of fluid mechanics problems. *Comput. Methods Appl. Mech. Eng.* **1996**, *139*, 315–347.
8. Onate, E.; Perazzo, F.; Miquel, J. A finite point method for elasticity problems. *Comput. Struct.* **2001**, *79*, 2151–2163.
9. Liu, M.B.; Liu, G. Smoothed particle hydrodynamics (SPH): An overview and recent developments. *Arch. Comput. Methods Eng.* **2010**, *17*, 25–76.
10. Mukherjee, Y.X.; Mukherjee, S. On boundary conditions in the element-free Galerkin method. *Comput. Mech.* **1997**, *19*, 264–270.
11. Ma, H.; Chen, J.; Deng, J. Analysis of the dynamic response for Kirchhoff plates by the element-free Galerkin method. *J. Comput. Appl. Math.* **2024**, *451*, 116093.
12. Boroomand, B.; Tabatabaei, A.A.; Onate, E. Simple modifications for stabilization of the finite point method. *Int. J. Numer. Methods Eng.* **2005**, *63*, 351–379.
13. Ferreira AJ, M.; Roque CM, C.; Martins PA, L.S. Analysis of composite plates using higher-order shear deformation theory and a finite point formulation based on the multiquadric radial basis function method. *Compos. Part B Eng.* **2003**, *34*, 627–636.
14. Li, S.; Huang, L.; Jiang, L.; Qin, R. A bidirectional B-spline finite point method for the analysis of piezoelectric laminated composite plates and its application in material parameter identification. *Compos. Struct.* **2014**, *107*, 346–362.
15. Lian, Y.P.; Zhang, X.; Liu, Y. Coupling of finite element method with material point method by local multi-mesh contact method. *Comput. Methods Appl. Mech. Eng.* **2011**, *200*, 3482–3494.
16. Shen, L.; Lv, G.; Shen, Z. A finite point method based on directional differences. *SIAM J. Numer. Anal.* **2009**, *47*, 2224–2242.
17. Liu, P.; Lin, K.; Liu, H.; Qin, R. Free transverse vibration analysis of axially functionally graded tapered Euler-Bernoulli beams through spline finite point method. *Shock Vib.* **2016**, *2016*, 5891030.
18. Shojaei, A.; Mudric, T.; Zaccariotto, M.; Galvanetto, U. A coupled meshless finite point/Peridynamic method for 2D dynamic fracture analysis. *Int. J. Mech. Sci.* **2016**, *119*, 419–431.
19. Ugural, A.C. *Stresses in Plates and Shells*; McGraw Hill: Boston, MA, USA, 1999.
20. Timoshenko, S. *Theory of Plates and Shells*; McGraw Hill: New York, NY, USA, 1959.
21. Rockafellar, R.T. Lagrange Multipliers and Optimality. *SIAM Rev.* **1993**, *35*, 183–238.

22. Clark, B.W.; Anderson, D.C. The penalty boundary method. *Finite Elem. Anal. Des.* **2003**, *39*, 387–401.
23. Krongauz, Y.; Belytschko, T. Enforcement of essential boundary conditions in meshless approximations using finite elements. *Comput. Methods Appl. Mech. Eng.* **1996**, *131*, 133–145.